STRENGTH PREDICTION OF ADHESIVELY-BONDED SCARF REPAIRS IN COMPOSITE STRUCTURES UNDER BENDING

R. D. S. G. Campilho[1,a], M. F. S. F. de Moura[1,b], A. M. G. Pinto[2,c], D. A. Ramantani[1,d], J. J. L. Morais[3,e], J. J. M. S. Domingues[2,f]

[1] FEUP, Faculdade de Engenharia da Universidade do Porto, R. Dr. Roberto Frias, s/n, 4200-465 Porto, Portugal

[2] ISEP, Instituto Superior de Engenharia do Porto, R. Dr. António Bernardino de Almeida, 431, 4200-072 Porto, Portugal

[3] CITAB/UTAD, Departamento de Engenharias, Quinta de Prados, 5001-801 Vila Real, Portugal

[a]raulcampilho@hotmail.com, [b]mfmoura@fe.up.pt, [c]agp@isep.ipp.pt, [d]dimitraramantani@hotmail.com, [e]jmorais@utad.pt, [f]jsd@isep.ipp.pt

Keywords: Cohesive Damage Model, Finite Element Method, Strength Prediction, Composite Repair.

Abstract. This work reports on the experimental and numerical study of the bending behaviour of two-dimensional adhesively-bonded scarf repairs of carbon-epoxy laminates, bonded with the ductile adhesive Araldite 2015®. Scarf angles varying from 2 to 45º were tested. The experimental work performed was used to validate a numerical Finite Element analysis using ABAQUS® and a methodology developed by the authors to predict the strength of bonded assemblies. This methodology consists on replacing the adhesive layer by cohesive elements, including mixed-mode criteria to deal with the mixed-mode behaviour usually observed in structures. Trapezoidal laws in pure modes I and II were used to account for the ductility of the adhesive used. The cohesive laws in pure modes I and II were determined with Double Cantilever Beam and End-Notched Flexure tests, respectively, using an inverse method. Since in the experiments interlaminar and transverse intralaminar failures of the carbon-epoxy components also occurred in some regions, cohesive laws to simulate these failure modes were also obtained experimentally with a similar procedure. A good correlation with the experiments was found on the elastic stiffness, maximum load and failure mode of the repairs, showing that this methodology simulates accurately the mechanical behaviour of bonded assemblies.

Introduction

Carbon-Fibre Reinforced Plastic (CFRP) composites are often used in structures requiring high specific strength and stiffness. However, these materials are highly susceptible to suffer delamination damage, due to their low interlaminar strength. Adhesively-bonded repairs of structures with these materials are increasing in engineering applications, compared to the traditional repair techniques, such as riveting or mechanical fastening. Adhesively-bonded repairs benefit from a reduction of weight, easy conformance to complex shapes, less stress concentrations, preservation of the fibres continuity, amongst other advantages. There are mainly two repair techniques for composite structures: strap (single or double) and scarf repairs. The larger bond areas and the reduction of stress concentrations at the bond edges due to the adherend tapering effect justify the higher efficiency of the scarf repairs, compared to the easy-execution strap repairs.

The majority of the works on the strength of scarf joints or repairs focus on their tensile behaviour. Li et al. [1] proposed a technique based on relative strain measurements, using Bragg grating sensors, to identify debonding onset in scarf joints under tension. Debonding onset was detected by a differential strain approach, using two sensors whose strain differential increased with the debond length. A two-dimensional stress and failure Finite Element Method (FEM) numerical analysis of

tensile loaded CFRP scarf repairs was carried out by Odi and Friend [2], for scarf angles varying from 1.1 to 9.2º. The repairs strength was predicted using the Tsai-Wu and maximum stress failure criteria for the adherend and the average shear stress failure criterion for the adhesive. Kumar et al. [3] presented an experimental and FEM study regarding the tensile strength of CFRP scarf joints. The numerical failure loads as a function of the scarf angle were obtained using the FEM and the Hashin-Lee criterion for the adherends, and agreed with the experimental ones.

This work addresses an experimental and numerical study of CFRP adhesively-bonded scarf repairs under bending. Scarf angles (α) varying from 2 to 45º are considered. The experimental results were used to validate a developed numerical methodology using the FEM and a mixed-mode cohesive damage model implemented in ABAQUS®. The behaviour of the adhesive layer was modelled using cohesive elements with trapezoidal traction-separation laws in pure modes I and II. This shape was selected to account for the ductility of the adhesive used in this work (Araldite® 2015). The respective cohesive laws in pure modes I and II were determined with Double Cantilever Beam (DCB) and End-Notched Flexure (ENF) tests, respectively, using an inverse method. Since in the experiments interlaminar and transverse intralaminar failures also occurred, cohesive laws to simulate these failure modes were also obtained experimentally with an identical procedure.

Cohesive Damage Model

Model Description. A mixed-mode (I+II) cohesive damage model implemented within zero thickness interface finite elements was used to simulate a thin adhesive layer of Araldite® 2015. A trapezoidal law between stresses ($\boldsymbol{\sigma}$) and relative displacements ($\boldsymbol{\delta}_\mathbf{r}$) between homologous points of the interface finite elements was used (Fig. 1).

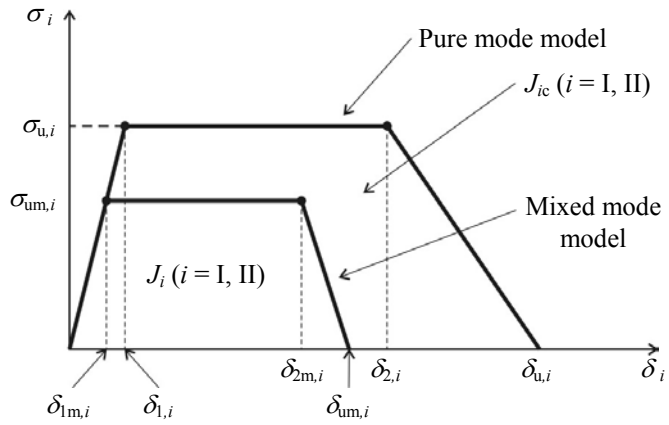

Fig. 1 – Trapezoidal softening law in pure mode and mixed mode.

It is thus necessary to know the local strength at the crack tip ($\sigma_{u,i}$, i=I, II) and the fracture toughness (J_{ic}, i=I, II) in each mode. Damage initiation is predicted using the following quadratic stress criterion

$$\begin{aligned} &\left(\frac{\sigma_{\mathrm{I}}}{\sigma_{\mathrm{u,I}}}\right)^2+\left(\frac{\sigma_{\mathrm{II}}}{\sigma_{\mathrm{u,II}}}\right)^2=1 \quad \text{if} \quad \sigma_{\mathrm{I}}>0 \\ &\sigma_{\mathrm{II}}=\sigma_{\mathrm{u,II}} \qquad\qquad\quad \text{if} \quad \sigma_{\mathrm{I}}\le 0 \end{aligned}, \tag{1}$$

where σ_i, (i=I, II) corresponds to the stress in a given integration point of an interface element in the respective pure mode. Stress softening onset is predicted by a quadratic displacements criterion similar to Eq. 1:

$$\left(\frac{\delta_{2\mathrm{m,I}}}{\delta_{2,\mathrm{I}}}\right)^2+\left(\frac{\delta_{2\mathrm{m,II}}}{\delta_{2,\mathrm{II}}}\right)^2=1. \tag{2}$$

$\delta_{2,i}$ (i=I, II) represent the relative displacements in each pure mode at the initiation of stress softening and $\delta_{2\mathrm{m},i}$ (i=I, II) the corresponding mixed-mode displacements. Damage growth is predicted using the linear energetic criterion

$$\frac{J_{\mathrm{I}}}{J_{\mathrm{Ic}}}+\frac{J_{\mathrm{II}}}{J_{\mathrm{IIc}}}=1. \tag{3}$$

The area under the minor trapezoid of Fig. 1 represents the energy released in each mode, while the bigger trapezoid area corresponds to the respective J_{ic}. When Eq. 3 is satisfied, damage propagation occurs and stresses are completely released, with the exception of normal compressive ones. A detailed description of the model used is presented in the work of Campilho et al. [4].

Cohesive Parameters. The adhesive layer was modelled numerically using the interface finite elements with the trapezoidal shape traction-separation laws described previously, instead of the solid finite elements typically employed to this end. The initial relationships between σ and δ_r in pure mode I and II, for $\delta<\delta_{1,i}$ (Fig. 1), are defined by the stiffness parameters (e_i, i=I, II), to simulate the elastic behaviour of the adhesive layer. Thus, these parameters are obtained by the ratio between the longitudinal or shear modulus (E or G, respectively) and the adhesive layer thickness (t_A). The values of E and G were determined experimentally [5] with bulk tensile tests and Thick Adherend Shear Tests (TAST), respectively (E=1850 MPa, G=650 MPa). To completely characterize the trapezoidal laws in pure modes I and II, the values of $\sigma_{u,i}$, $\delta_{2,i}$ and J_{ic} must also be determined. J_{ic} was obtained by conventional fracture characterization tests using the same value of t_A of the specimens to be simulated, using DCB and ENF tests for pure mode I and II, by the respective order. The two other parameters were calculated by an inverse method with these same tests. Using this methodology, the value of J_{ic} is used as an input parameter in numerical DCB or ENF models. These models, having the individual dimensions of each tested specimen, include the respective pure mode cohesive law with the value of J_{ic} previously determined for the respective specimen and typical values for $\sigma_{u,i}$ and $\delta_{2,i}$. These properties are determined performing a few iterations until a good accuracy between the experimental and numerical load-displacement (P-δ) curves is achieved. In these repairs, regions of composite interlaminar and intralaminar fractures were also detected. Consequently, the cohesive properties in pure modes I and II for these failures were also determined by a similar technique. However, in these situations, a penalty function method was used for the initial ascending part of the pure mode I and II cohesive laws, since the interface finite elements simulate a zero thickness interface instead of a finite thickness layer. Moreover, triangular traction-separation laws were used, due to the brittle nature of these interfaces. Failure of the composite plies in the fibres direction was also taken into account, even though this was not detected experimentally. The detailed explanation of the inverse methodology and the determination of the adhesive layer, composite interlaminar, intralaminar and fibre cohesive parameters are presented in a previous work [6]. For the adhesive layer laws, it is emphasized that cohesive failures were always obtained in the DCB and ENF specimens, which is essential to characterize the adhesive layer accurately.

Experimental Work

The geometry of the scarf repairs is presented in Fig. 2 (a) (a=270 mm, b=15 mm, t_P=2.4 mm, t_A=0.2 mm and d=10 mm). Values of α of 2, 3, 6, 9, 15, 25 and 45º were evaluated. Smaller scarf angles were not tested, since the repair lengths needed were not compatible with the chosen value of α. Fig. 2 (b) shows the test setup, with S=250 mm, S'=150 mm, d_c=5 mm and e=10 mm. The laminates and patches were fabricated using carbon/epoxy prepreg (Texipreg HS160RM from SEAL®) with 0.15 mm of ply thickness and a $[0_2,90_2,0_2,90_2]_S$ lay-up. The orthotropic elastic properties of a unidirectional lamina are presented in [7]. A detailed description of the specimens fabrication procedure is given in the work of Campilho et al. [6].The bending tests were performed with an electro-mechanical Instron® 5848 Microtester equipped with a 2kN load cell. A constant velocity was applied (2 mm/min) during the experimental tests, accomplished at room temperature. A sample rate of 5 points per second was used. Six specimens were tested for each value of α and at least four valid results were always obtained.

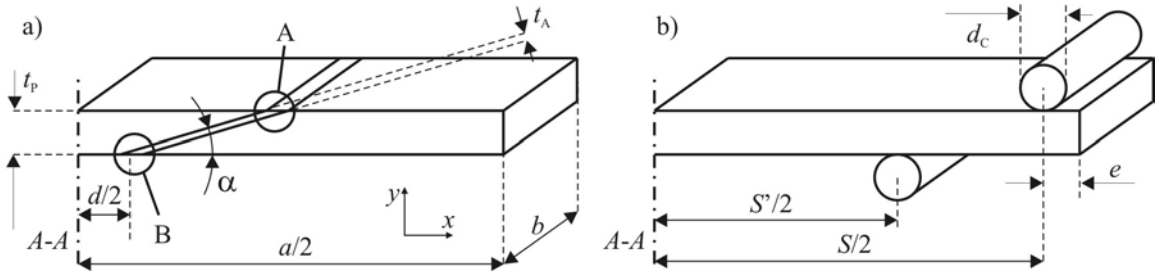

Fig. 2 – Scarf repair geometry (a) and test setup (b).

Numerical Work

The numerical analysis, including the interface finite elements with different cohesive laws for damage onset propagation, was performed in ABAQUS®, including geometrical and material non-linearities. The laminates and patches were modelled with plane-stress 8-node rectangular and 6-node triangular solid finite elements. Fig. 3 (a) shows a detail of the mesh at the lower scarf tip (region B in Fig. 2 (a)), for the α=25º repair. Eighty solid finite elements were used along the bond length near the adhesive layer, due to the high stress gradients in this region. Due to the symmetry of these repairs, only half the specimen was considered, applying symmetry conditions at the middle of the repair (line A-A in Fig. 2). The placement of the interface finite elements is presented in Fig. 3 (b). The adhesive layer elements were placed along the bond length replacing the adhesive layer, the interlaminar elements were positioned between differently oriented plies, the transverse intralaminar elements were used vertically in the 90º plies to simulate the intralaminar matrix cracking and the fibre elements were placed vertically in the 0º plies to simulate fibre cracking.

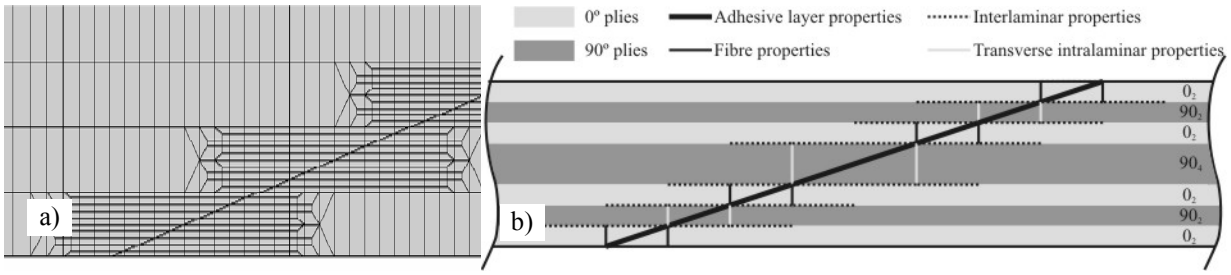

Fig. 3 – Scarf repair mesh for the α=25º repair (a) and interface finite elements loci (b).

Results

An identical failure mode of the repairs was found experimentally for all values of α, consisting on a mixed cohesive and interlaminar/intralaminar failure of the laminate at the scarf region. Fig. 4 (a) and (b) correspond to the experimental and numerical failures, respectively, for the α=25º repair. This failure can be described as a cohesive failure along the bond length, except at the two sets of 90º plies nearest the lower scarf tip (region B in Fig. 2 (a)). For these, a mixed interlaminar/intralaminar failure of the laminate occurred. This behaviour was captured by the numerical simulations. Fig. 5 (a) and (b) compare the experimental and numerical P-δ curves for the α=6º and α=25º repairs, respectively. The numerical simulation predicted accurately the stiffness (K) and maximum load (P_m) for these repairs. A slight difference was observed on P_m for the bigger values of α (including the α=25º repair, Fig. 5 (b)).

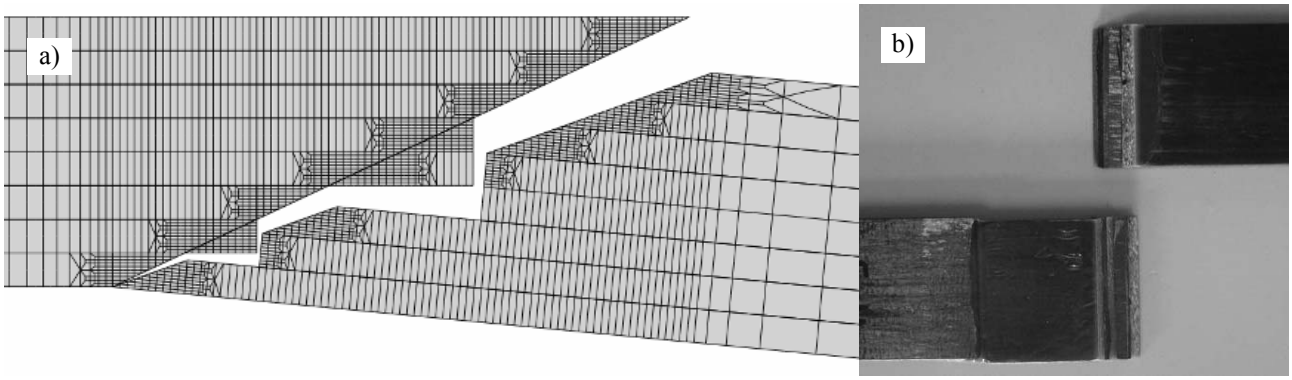

Fig. 4 – Experimental (a) and numerical (b) fractures for a α=25º repair.

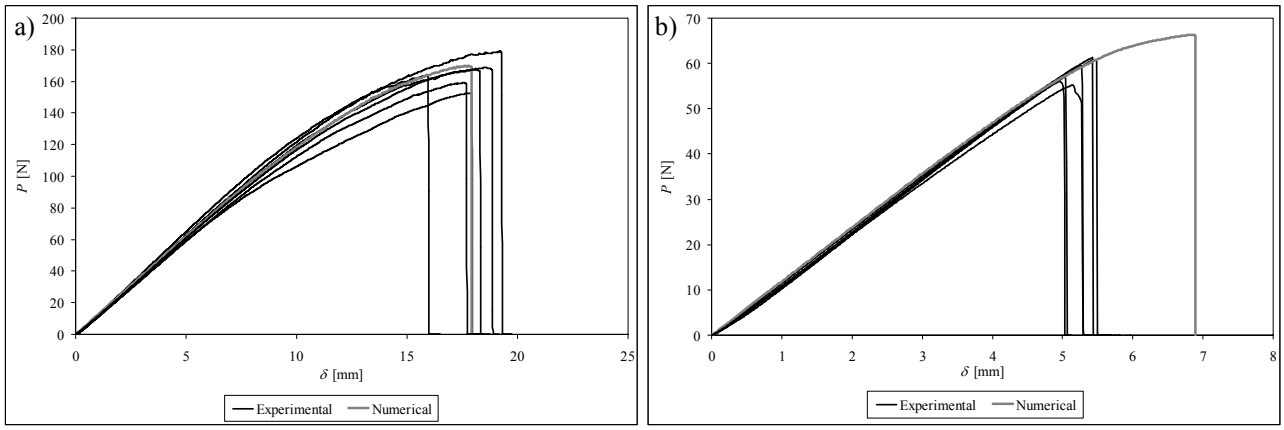

Fig. 5 – Experimental and numerical P-δ curves comparison for the α=6º (a) and α=25º (b) repairs.

The average results of the tests and respective FEM predictions are summarized in terms of K (Fig. 6 (a)) and P_m (Fig. 6 (b)). The standard deviation of the experiments is also included. A small increasing trend of K was observed with the reduction of α. This tendency was also obtained numerically, although a non-negligible difference was detected for the α=3º repair. Small variations of t_A are the probable explanation for this inconsistency. The values of P_m showed an exponential increase with the reduction of α. This is explained by the corresponding reduction of the adhesive layer stresses magnitude, due to the laminates and patches higher flexibility at the scarf region. Also in this situation the numerical simulations reproduced the experiments accurately. Based on the results presented here, the α=2º and α=3º repairs are recommended, since they lead to the bigger values of P_m. The good overall agreement between the experimental and numerical results allows emphasizing the suitability of the proposed methodology to predict the fracture behaviour of these bonded assemblies.

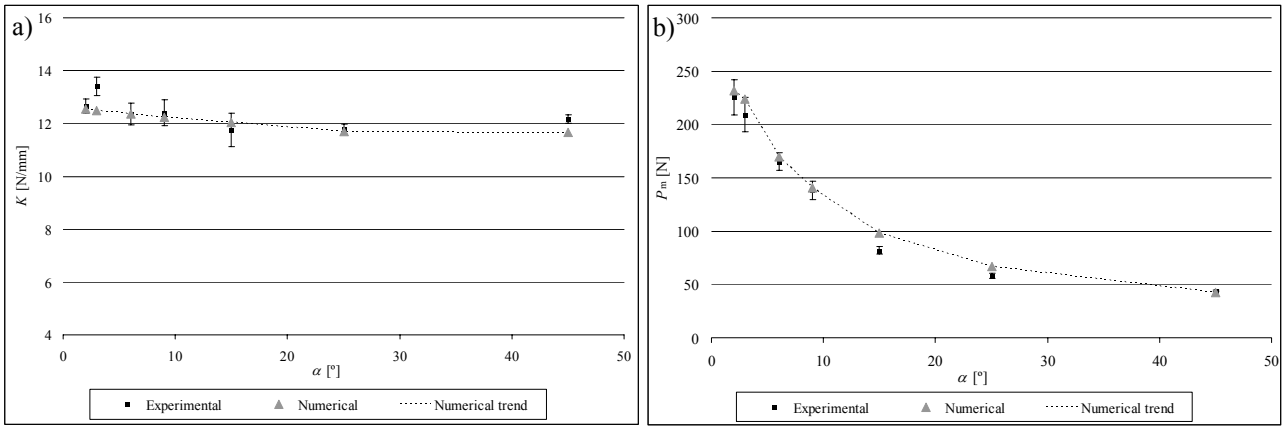

Fig. 6 – K as a function of α (a) and P_m as a function of α (b).

Summary

In this work, a numerical methodology was presented to predict the mechanical behaviour of bonded assemblies. A mixed-mode (I+II) cohesive damage model with trapezoidal shape laws was employed to simulate the adhesive layer behaviour. The methodology was extended to simulate the interlaminar, intralaminar and fibre fracture of the composite laminates and patches, to fully reproduce the experimental failure modes. The different traction-separation laws were determined using an inverse method, which consisted in obtaining the fracture toughness in pure modes I and II with Double-Cantilever Beam and End-Notched Flexure tests, respectively, and estimating the other parameters of the pure mode laws using a fitting iterative procedure between the experimental and numerical load-displacement curves. The mixed-mode behaviour of the adhesive layer or within the composite, typical in these assemblies, was simulated with appropriate criteria. This numerical methodology was validated experimentally with carbon-epoxy scarf repairs under bending, for different scarf angles. The comparison was performed in terms of the repairs elastic stiffness, the maximum load, as well as the failure path until complete failure. The results obtained allowed concluding that the methodology presented in this work is adequate to simulate the mechanical behaviour of bonded assemblies.

References

[1] H.C.H. Li, F. Beck, O. Dupouy, I. Herszberg, P.R. Stoddart, C.E. Davis and A.P. Mouritz: Composite Struct. Vol. 76 (2006), p. 234.

[2] R.A. Odi and C.M. Friend: Int. J. Adhesion Adhesives Vol. 24 (2004), p. 389.

[3] S.B. Kumar, I. Sridhar, S. Sivashanker, S.O. Osiyemi and A. Bag: Mater. Sci. Eng. B Vol. 132 (2006), p. 113.

[4] R.D.S.G. Campilho, M.F.S.F. de Moura and J.J.M.S. Domingues: Int. J. Solids Struct. Vol. 45 (2008), p. 1497.

[5] E.A.S. Marques and L.F.M. da Silva: J. Adhesion Vol. 84 (2008), p. 917.

[6] R.D.S.G. Campilho, M.F.S.F. de Moura, A.M.G. Pinto, J.J.L. Morais and J.J.M.S. Domingues: Composites Part B: Eng. Vol. 40 (2009), p. 149.

[7] R.D.S.G. Campilho, M.F.S.F. de Moura and J.J.M.S. Domingues: Composites Sci. Technol. Vol. 65 (2005), p. 1948.